

# We are IntechOpen, the world's leading publisher of Open Access books Built by scientists, for scientists

4,800

Open access books available

122,000

International authors and editors

135M

Downloads

Our authors are among the

154

Countries delivered to

TOP 1%

most cited scientists

12.2%

Contributors from top 500 universities



WEB OF SCIENCE™

Selection of our books indexed in the Book Citation Index  
in Web of Science™ Core Collection (BKCI)

Interested in publishing with us?  
Contact [book.department@intechopen.com](mailto:book.department@intechopen.com)

Numbers displayed above are based on latest data collected.  
For more information visit [www.intechopen.com](http://www.intechopen.com)



# Blast Effects on Structural Elements

*María Chiquito, Anastasio P. Santos, Lina M. López  
and Ricardo Castedo*

## Abstract

Blast loads can represent a great hazard to existing structures. Their effects on structural elements can be decisive for the integrity of both the structure itself and the people within it. The behaviour of the individual elements of a building is totally different due to the heterogeneity of the materials composing them. This fact makes it necessary to carry out tests on each type of structural element in order to correctly evaluate the response of the structure. In addition, the scale effect can produce inaccurate results, making it necessary for tests to be performed on a full scale to validate the results. In this work, the results of several tests with explosives are presented, in different constructive elements, all of them carried out at full scale. These elements range from the structural elements (beams and concrete slabs) to the weak elements of a building (masonry panels).

**Keywords:** blast load, full scale, numerical modelling, damage assessment, structural elements

## 1. Introduction

In the last decades, the number of terrorist attacks made through explosive loads has increased notably. In this scenario, not only military or government facilities are targeted, but any kind of civil building may also be attacked. This fact has revealed the vulnerability of structures to explosions and blast waves and, hence, the hazard for human lives. Understanding the behaviour of structures against blast loads is absolutely essential to improve their safety.

When an explosion occurs, a sudden release of energy to the atmosphere results in a transient pressure wave or blast wave. Many structures may experience some degree of damage from air blast when the overpressure in the blast wave is about 3–5 kPa or more. The blast wave propagates outwards in all directions from the source at supersonic speed. The shock wave is characterised by an instant rise in pressure from ambient atmospheric pressure  $P_0$  to a peak incident overpressure  $P_{so}$ . From the incident peak, the overpressure decays exponentially to the ambient value. This is the positive phase duration which is followed by a blast wind of negative pressure which sucks items back in towards the centre. This negative phase is usually much longer than the positive phase. Because negative pressures are relatively small compared with the positive phase, they are not commonly considered in blast-resistant design.

Terrorist attacks on structures may not be eliminated completely, but the effects of these attacks can be mitigated. Several techniques have been developed in recent

years for this purpose, such as retrofitting or coating applications [1, 2], internal reinforcement [3, 4] or geometrical modifications in buildings [5]. It is desirable that mitigation techniques may be applied in both new and existing buildings.

The behaviour of the individual elements of a building is totally different from each other due to the heterogeneity of the materials composing them. This fact makes it necessary to carry out tests on each type of structural element in order to correctly evaluate the structure response. The behaviour of structural elements is completely different from the response of weak elements, although all of them have an influence on each other. In addition, the scale effect can produce inaccurate results, making it necessary for tests to be performed at full scale [6–8]. Furthermore, a certain repetitiveness is required to validate the results.

Due to the high costs of this kind of test, many studies in the last years have been done based on numerical modelling [finite element (FE) analysis]. However, when working in the determination of the response of structures subjected to blast loading, the complexity of the problem makes field tests mandatory to validate the results and calibrate analytical models, extending the limited scope of the field data to other design situations [9, 10].

In this work the results of tests with explosives against different constructive elements are presented, all of them carried out at full scale. These elements range from the structural elements (beams and concrete slabs) to the weak elements of a building (masonry panels). In all cases, the study carried out includes field tests, damage assessment and numerical modelling.

## **2. Analysis methodology**

For a complete analysis of the different structural elements, the work is divided in three different and complementary stages:

- A field test campaign, always developed at full scale
- A damage assessment based on analytical and visual methods
- A numerical simulation to compare the results obtained in field tests

### **2.1 Test campaign**

The field test campaign is designed depending on the structural element to be analysed. A previous work is carried out to calibrate particular parameters such as scaled distance, standoff distance or height of the charge. Due to the uncertainties in this kind of tests, sometimes it is necessary to correct a specific parameter along the tests to obtain the desired result. The best result to get as much information as possible from the test is to produce an intermediate damage. When a structure collapses, no information can be extracted after the explosion. The same happens when damage is minimum. Therefore, an intermediate level of damage is the best option to analyse blast effects on structures.

Elements to be tested are constructed with a representative size to avoid the scale effect. Boundary conditions are reproduced as similar as possible to a real situation. To analyse the improvement of different retrofitting materials, a non-reinforced element is always tested as a “control element”. The explosive used in the tests to be reported below was PG2, a RDX-based (86%) plastic explosive for military use (similar to C4), with experimental TNT equivalent based on impulse of 0.86 [11].

Several parameters are measured in tests to characterise the explosion. Tests are monitored with pressure gauges, accelerometers, high-speed cameras, conventional cameras, laser scanner where possible or equipment to measure the velocity of detonation of the explosive with a high-speed recording device. These data are then used to calibrate the numerical simulation.

After the test, a series of measurements are collected for further analysis: the rebound value measured with a Schmidt hammer following a methodology developed by [12] combined with the surface damaged area, the spalling mass, the length of cracks and displacements.

## 2.2 Damage assessment

Considering all the data collected in field tests, a damage evaluation is made combining visual observations and analytical methods. The combination of both methods allows to establish a classification of damage which ranges from moderate damage to collapse. Visual observations provide information about the condition of the specimen after the explosion such as cracks, failure patterns, debris, etc. However, this kind of analysis does not allow to check if there is internal damage. To fill this gap, as analytical method, a methodology based on the rebound principle with a Schmidt hammer is used.

### 2.2.1 Damage based on rebound number

Methods based on the rebound principle consist of measuring the rebound of spring-driven hammer after its impact with the material surface to check its uniformity. For damage evaluation, the objective is to find a variation in the rebound number after a blast event and not a direct strength correlation [12]. For this purpose, a series of measurements on the specimen are done. One measurement location point is defined by 12 points inside a template: six for the evaluation before and six for the evaluation after the explosion (see **Figure 1** for details).  $Q_1$  is the median of the six points evaluated before test  $B_i$  (suffix  $i$  being the corresponding number that goes from 1 to 6), and  $Q_2$  is the median for the points after test  $A_i$ . Both medians are then compared using the Wilcoxon rank-sum test. A p-value lower than 0.05 may confirm a decrease in the rebound number after the explosion with a 95% confidence level, and hence the point analysed is damaged.

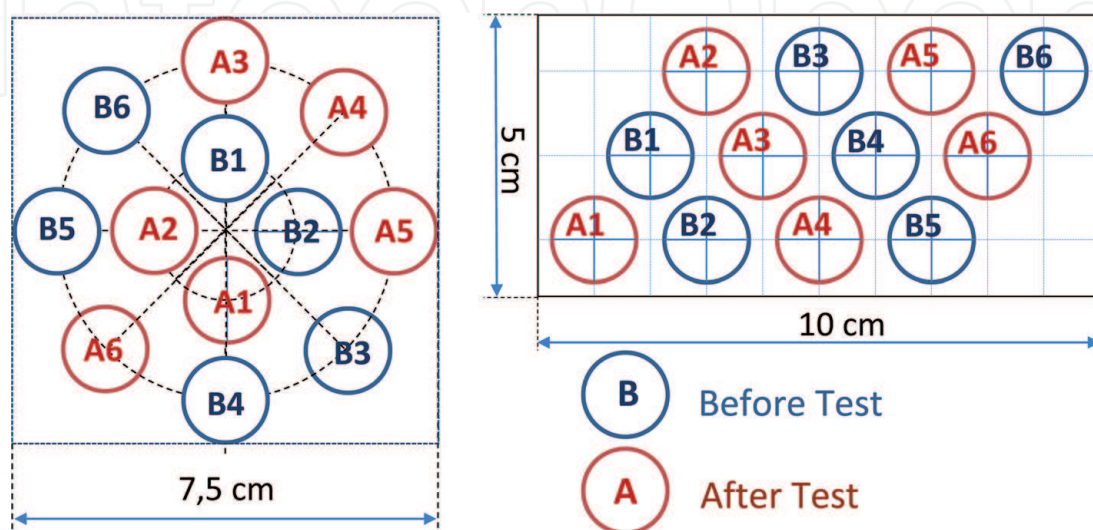


**Figure 1.** Models of templates used to measure the rebound number. Left, point template used for slabs; right, point template used for bricks.

For this purpose, damage  $d$  is defined as

$$\begin{aligned} d &= 1 - \frac{Q_2}{Q_1}, \text{ if } p \leq 0.05 \\ d &= 0, \text{ if } p > 0.05 \end{aligned} \quad (1)$$

Damage ranks from 0 to 1, 1 being a damage of 100%. In order to complete the damage analysis and based on the results obtained, a damage or contour map is created. For this purpose, a grid of 200 linearly spaced points is created for each specimen at each direction (horizontal and vertical). Then, a fitting surface to the data with a triangle-based cubic interpolation already implemented in MATLAB is calculated and plotted. With this data, a parameter called global damage ( $d_{200}$ ) is obtained. This parameter is calculated with the mean of the 200 points of the grid. With this parameter, an overestimation of the mean damage is reduced.

### 2.2.2 Relative area of damage and crack lengths

To complete the damage evaluation, two parameters related to the surface damage can be used to rank the structure's behaviour, based on visual inspection and not in damage maps (or Schmidt hammer data). The relative damaged area ( $d_A$ ) is defined as the ratio of the surface with total damage (damage equal to 1) over the total surface of the specimen. The crack length, defined as the sum of the length of all cracks presented on the specimen, can be used as another additional parameter for damage evaluation.

### 2.2.3 Spalling mass

After a blast event, fragmentation is the major source of wounds when the structure does not collapse. The mass of debris and the distance to which they are projected can be used as a potential damage parameter of the explosion. Therefore, the spalling fragments are classified and weighted after the tests. As this parameter is only obtained in some tests, a general comparison and conclusions with rebound data are not possible.

### 2.2.4 Displacements

In order to obtain more information about the structure's behaviour, tests are monitored, whenever possible, with a laser scanner measuring the geometry before and after the event. In other cases, the maximum deflection of the element, at the end of the test, is measured to assess the final degree of damage.

## 2.3 Numerical modelling

The destructive result of the test together with the short duration of both blast loading and response of the structure limits the opportunity for a depth understanding of the processes involved. Therefore, the use of 3D full-scale finite element modelling is fundamental to understand, predict and simulate the failure mechanism and the damage area of structural elements against blasting. Numerical models are conducted using LS-DYNA software which is based on explicit numerical methods that are suitable for solving problems associated with the high velocities and large deformations induced by blast waves.

### 3. Structural elements

In this section, the results of tests with explosives are presented in different constructive elements, all of them carried out at full scale. In all cases, the study includes field tests, damage assessment and numerical modelling. All tests shown here were conducted at the Technological Institute of “La Marañosa”, part of the National Institute for Aerospace Technology (INTA), Spain.

#### 3.1 Masonry walls

A total of four masonry walls tested in two different trials are included in this chapter. The walls were built inside a concrete structure, simulating the real situation of a building. For each shot two boxes or rooms (box A and box B in **Figure 2**) were built with 40 cm × 20 cm × 20 cm masonry concrete blocks joined with standard mortar. For the frontal wall, exposed to the explosion, 40 cm × 20 cm × 15 cm blocks were used. Inner dimensions of each box were 3 m × 3 m × 3 m with a 1 m separation between boxes (see **Figure 2**). Lateral and back walls were reinforced filling the hollows with mortar and steel bars (B 500S) evenly spaced in horizontal and vertical directions. The frontal wall was a continuous wall, covering the space between boxes and projecting 1 m at both sides in order to increase the impulse load over the wall. Both rooms had an access door by the central corridor. Different coatings were implemented inside the rooms for debris assessment. In each box, the inner face of the masonry wall was partially tiled (a little more than half), and the rest was pointed. After the first test, the frontal wall was rebuilt for the second trial. Explosive mass was 5 kg eq TNT and was located 0.96 m over the ground at a standoff distance of 5 m ( $2.92 \text{ m/kg}^{1/3}$ ) to the front wall.

The solution tested for each box was:

- Test M1, box A (M1A): non-reinforced wall for comparison
- Test M1, box B (M1B): aluminium mesh anchored to the external face of the wall and exposed to the explosion



**Figure 2.**  
 Test setup and details.

- Test M2, box A (M2A): a glass fibre-reinforced sheet glued with a polyurethane adhesive in the external side of the wall
- Test M2, box B (M2B): a basalt fibre mesh attached with cementitious mortar to the inner face

### 3.1.1 Results and discussion

**Table 1** shows the main results obtained from the test instrumentation: pressure and impulses from pressure gauges and shockwave velocity from the high-speed video.

Transducers P1, P2 and P3 were measuring the reflected pressure, while P4 and P5 were measuring the side-on or incident pressure. P6 registered the peak pressure inside box B. It can be assumed that there are not substantial pressure variations in the vertical component because the triple point height at 5 m from the charge is higher than the wall height (>3 m). The results listed on **Table 1** are from Test M1 with the exception of gauge P6 that comes from Test M2. Measurements from transducers P1 to P5 for Test M2 were lost due to a failure of the acquisition system.

Pressure results are compared with the manual from the Department of Defence, USA, UFC3-340 (DoD, 2006) [13] values and represented versus scaled distances in **Figure 3A**.

The high-speed camera was located orthogonal to the shockwave advance, at a safe distance from the explosion. This position allows to analyse the shock front propagation and its reflection in the wall face. At both tests images were recorded at 8000 frames per second with a “FastCam Sa-3”, model 120 k C2, manufactured by Photron. **Figure 3B** shows the shockwave velocity evaluated compared with the values obtained from UFC 3-340.

**Figure 4A** shows the images of the outer face of the masonry walls after the test. Location of the boxes is marked with a discontinuous line. Damage with the rebound hammer was evaluated in 13 location points on each wall. Mean damage values obtained ( $d_{200}$ ) are listed in **Table 2**. Contour maps of damage have been represented in **Figure 4B**. External damage appears at the sides, lower part in M1A and upper left corner in M1B. In test M2B damage also occurs at the left side.

Test	Location	Distance	Scaled distance	Pressure	Impulse	Shock velocity
		m	m/kg <sup>1/3</sup>	kPa	kPa.ms	m/s
M1	P1	6.4	3.7	271	395	
M1	P2	5	2.9	386	501	
M1	P3	6.4	3.7	242	297	
M1	P4	5	2.9	149		
M1	P5	10	5.8	42	91	
M2	P6	12	7.0	5		
M1	u1	2.5	1.5			889
M1	u2	3.5	2.0			667
M2	u1	2.5	1.5			727
M2	u2	3.5	2.0			571

**Table 1.**  
Pressure gauge results and shockwave velocity measurements.

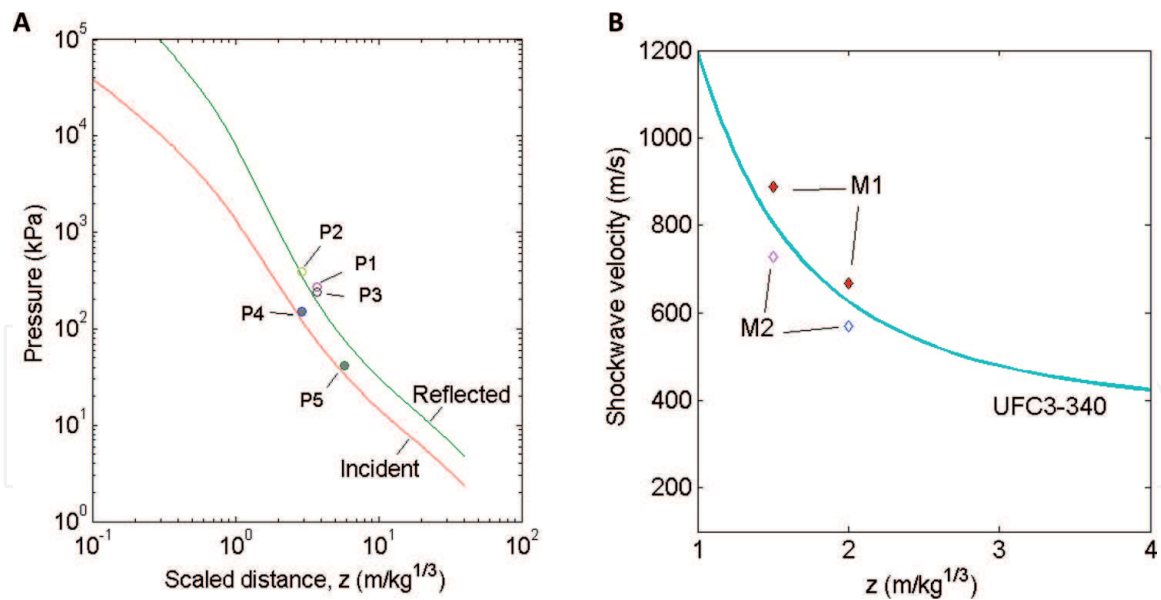


**Figure 3.**  
 (A) Pressure measurements compared with UFC3-340 data. (B) Shockwave velocity compared with UFC3-340 data.

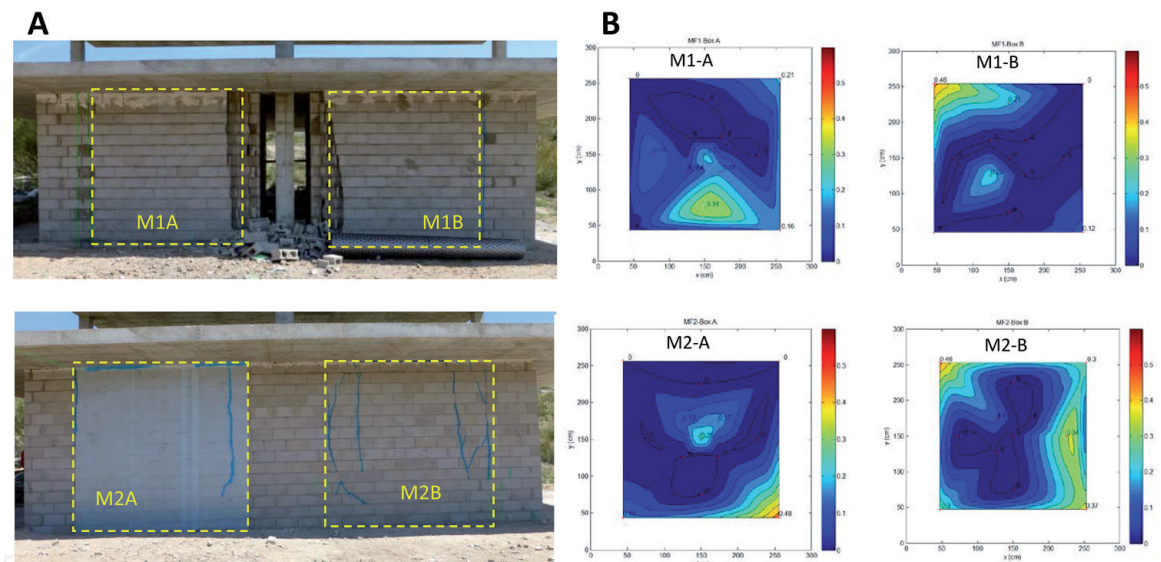


**Figure 4.**  
 (A) Results of external face of the walls after both tests. (B) Damage maps of the walls.

Test	Box	Solution	Fragment mass (kg)			Mean damage
			Total	Tiling area	Pointing area	
M1	A	No protection	63.4	56.6	6.8	0.08
M1	B	External metal mesh	39.5	37.4	2.0	0.04
M2	A	Glass fibre external film	24.8	23.5	1.3	0.08
M2	B	Basalt fibre inner film	1.7	0.8	0.9	0.14

**Table 2.**  
 Debris mass and mean damage obtained with the rebound hammer.

For fragment analysis, a grid was drawn on the floor inside the boxes as shown in **Figure 5**. As can be seen, debris mainly appear in the tiling zone. Referring to the debris collected, in Test M1, it was 63.4 kg inside box A and 39.5 kg inside box B. In



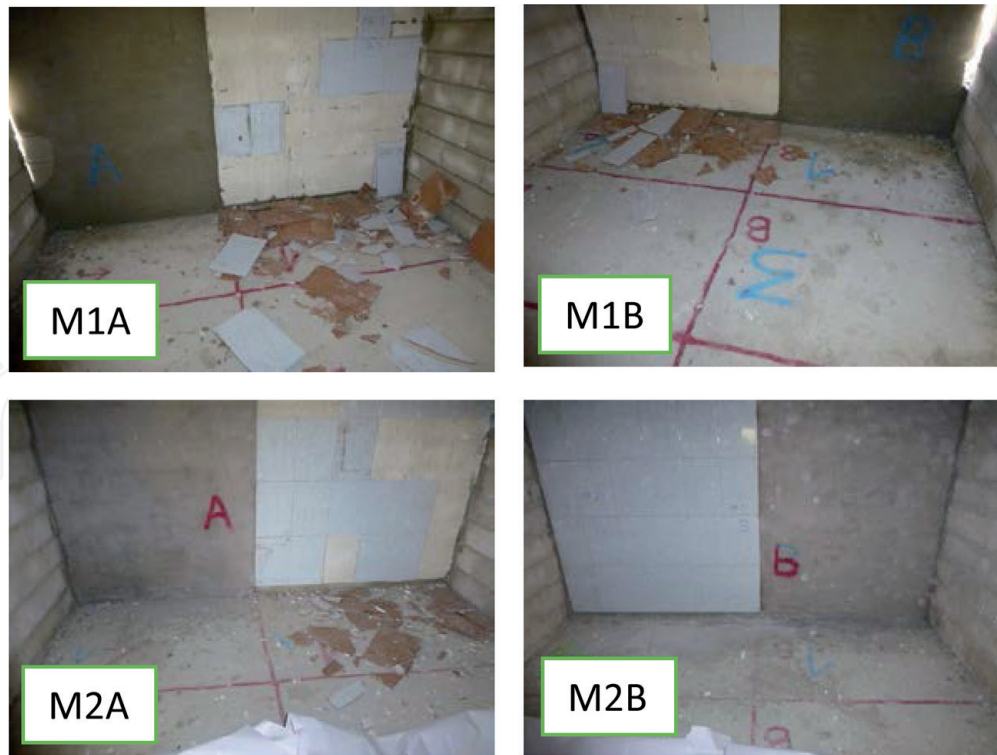


**Figure 5.**  
Fragments inside the boxes after the test.

Test M2, 24.8 kg of fragments were inside box A and 1.7 kg inside box B. **Table 2** shows the different fragment mass weighted at each box, specifying the mass collected inside the tiled zone and inside the pointing area. Note that in M2B there were hardly any fragments.

Comparing the results from box A with box B at M1 test, wall M1B (with the metal mesh) appears with a lower mean damage (see **Figure 4B** and **Table 2**) as logic dictates because of the external protection. Furthermore, there is an important reduction in the spalling mass (from 63 kg in M1A to 40 kg in M1B).

Regarding Test M2, the influence of the external glass fibre film (M2A) and an inner basalt fibre film in wall M2B may be compared. The external film (M2A) produces a decrease on the mean damage compared with M2B, and there is a strong reduction of debris due to the inner basalt fibre film in wall M2B (from 25 kg in M2A to 1.7 kg in M2B).

Results from test one cannot be compared with those of the second test. This is due to the difference in the lapse time between the construction and test which was higher for the second. This alteration means that the results cannot be extrapolated.

### 3.2 Slabs and beams

Considering structural elements, different beams and slab were tested and analysed (see **Table 3** for details). The test acronym is formed by a letter that refers to the specimen to be tested as follows, S for slabs and B for beams, followed by a correlative number that reflects the trial number. Different solutions were implemented and detailed in **Table 3**. The charge mass, in terms of TNT equivalent, ranged from 2 (spherical shape) to 15 kg (cubic shape). The detonator used to initiate the explosive was located at the centre of the charge. The scaled distance went from 0.2 up to  $0.79 \text{ m/kg}^{1/3}$  for slabs and beam tests.

For slabs, nine specimens of  $4.40 \text{ m} \times 1.50 \text{ m}$  and thickness of 0.15 m were built using a reinforced concrete with a nominal characteristic compressive strength

Test no.	Specimen	Description <sup>a</sup>	Standoff dist., R	Equiv. TNT, W	Scaled dist.
			m	kg	m/kg <sup>1/3</sup>
S1, S2, S3	Slab	RC	1	2	0.79
S4	Slab	RC	1	15	0.41
S5	Slab	RC	0.5	15	0.20
S6	Slab	RC-SSA	0.5	15	0.20
S7	Slab	RC-SSG	0.5	15	0.20
S8	Slab	SFRC	0.5	15	0.20
S9	Slab	PPFRC	0.5	15	0.20
B1, B2	Beam	RC	1	2	0.79
B3	Beam	RC	1	4	0.63
B4	Beam	RC	1	15	0.41
B5	Beam	RC	0.5	15	0.20

<sup>a</sup>RC, reinforced concrete; SSA, steel sheet anchored on top; SSG, steel sheet glued on top; SFRC, steel fibre-reinforced concrete; PPFRC, polypropylene fibre-reinforced concrete

**Table 3.**  
 Characteristics of the tests.

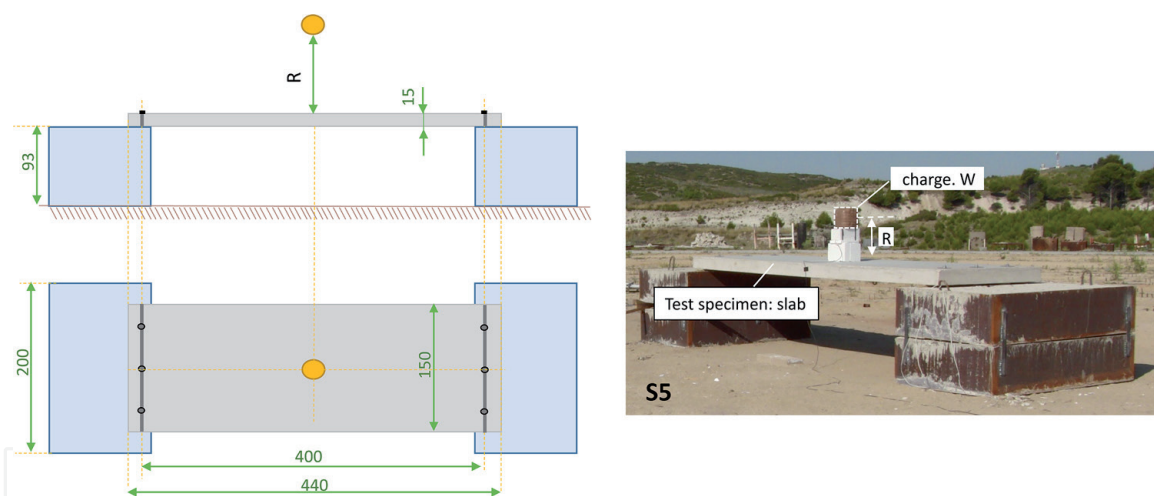


**Figure 6.**  
 Slab test setup.

of 25 MPa. Slabs were anchored at the edges to concrete blocks pretending a rigid support. **Figure 6** shows the test layout. The reinforced meshing was constructed with a 12 mm diameter rebar spaced 150 mm × 150 mm. In addition, some slabs had an extra reinforcement for protection purposes. In slabs S6 and S7, a steel sheet of 1.50 m × 1.50 m and a thickness of 10 mm were located on the surface directly exposed to the blast. Fibre-reinforced concrete was used in slabs S8 and S9. For S8 steel fibres were used and polypropylene fibres for S9. The main characteristics of concrete, steel and fibres used are detailed in **Table 4**.

The explosive charge for standoff distances of 1 m was located hanging from a rope, while for lower distances, the charge was placed on an expanded polystyrene cubic support. Note that the expanded polystyrene cube used for tests S4–S9 is just acting as a placeholder and the possibility of a shockwave reflection on the cube can be rejected.

In case of beams, five reinforced concrete specimens were tested. **Figure 7** shows the test setup and the charge placement. Beams had a section of 0.25 m × 0.20 m

	Concrete	Steel bars	Steel sheet	SFRC	PPFRC
Density (kg/m <sup>3</sup> )	2300	7850	7850	—	—
Compressive strength (MPa)	25	—	—	44.16	43.33
Tensile strength (MPa)	3.7	550	550	8.12	5.62
Young modulus (MPa)	$273 \times 10^2$	$200 \times 10^3$	$200 \times 10^3$	—	—
Yield strength (MPa)	—	500	275	—	—
Tangent modulus (MPa)	—	425	1850	—	—
Fibres dosage in concrete (kg/m <sup>3</sup> )	—	—	—	120 <sup>a</sup>	9 <sup>a</sup>
Length (mm)	—	—	—	$50 \pm 1^a$	$48 \pm 1^a$
Diameter (mm)	—	—	—	$1 \pm 0.1^a$	$0.84 \pm 0.1^a$
Specific volume fraction (%)	—	—	—	1.5 <sup>a</sup>	1 <sup>a</sup>

<sup>a</sup>Fibre properties

**Table 4.**  
List of materials' characteristics used in slabs and beams.

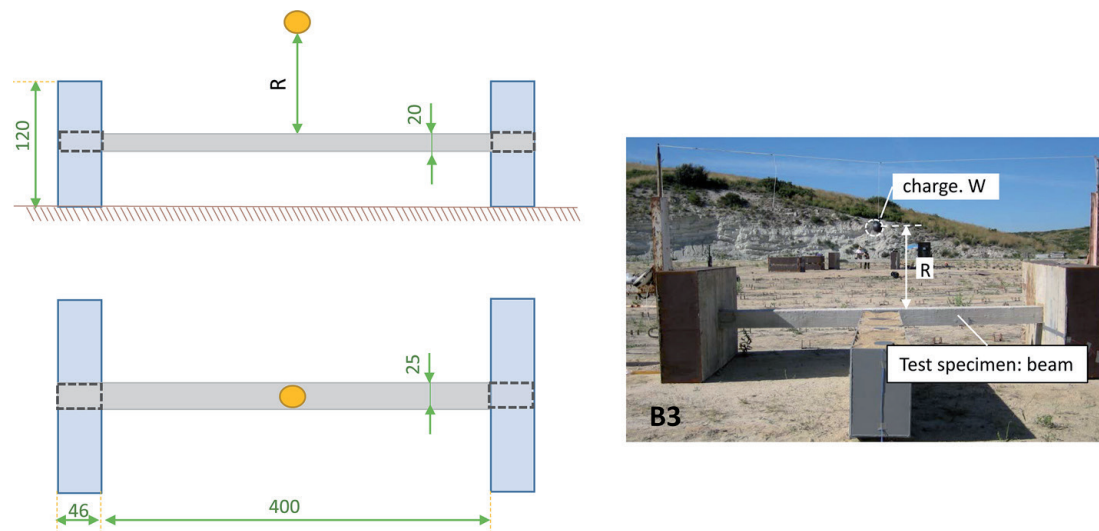


**Figure 7.**  
Beam test setup.

with spans of 4.00 m. The reinforcement consists of four holding bars of 12 mm in diameter and 6 mm diameter vertical stirrups spaced 150 mm along. The materials used here (concrete and steel) were the same than those used in the slabs (see **Table 4**). Each beam was fixed at both ends to a concrete block. For beams B1, B2 and B3, the explosive was hanged from a rope; however, for trial B4, the explosive was situated on an expanded polystyrene cubic support.

In order to assure the equipment integrity, measuring devices were only used in tests with low explosive charge (S1–S3 and B1, B2). To calibrate and validate numerical models, these data are necessary. Three accelerometers were used in each specimen and two pressure transducers with ablative protection. In these tests, high-speed camera resulted as not very useful as the “fire ball” covered all the screen, but information about the blast phenomena may be always extracted from videos.

### 3.2.1 Results and discussion

**Table 5** shows the different parameters of damage calculated. A rank is also included for the assessment result, based on authors' experience and others [3, 8, 10, 14, 15], and considering  $d_{200}$  and  $d_A$  parameters, no damage, moderate or severe.

Test no.	Scaled distance ( $\text{m/kg}^{1/3}$ )	Assessment result	Points $n$	Damage		Area damaged	
				$d_n$	$d_{200}$	$d_{A,top}$	$d_{A,bottom}$
S1, S2, S3	0.79	No damage	19	0.00	0.00	0	0
S4	0.41	Moderate	19	0.23	0.10	0.03	0.07
S5	0.20	Severe	19	0.38	0.27	0.07	0.27
S6	0.20	Severe	19	0.53	0.30	0.22	0.32
S7	0.20	Severe	19	0.42	0.25	0.11	0.28
S8	0.20	Severe	19	0.40	0.27	0.05	0.13
S9	0.20	Severe	19	0.48	0.28	0.06	0.15
B1	0.79	No damage	9	0.00	0.00	0	0
B2	0.79	No damage	9	0.01	0.00	0	0
B3	0.63	No damage	9	0.01	0.00	0	0
B4	0.41	Moderate	9	0.11	0.08	0.08	—
B5	0.20	Severe	9	0.37	0.22	0.20	—

**Table 5.**  
 Damage parameters for slabs and beam tests.

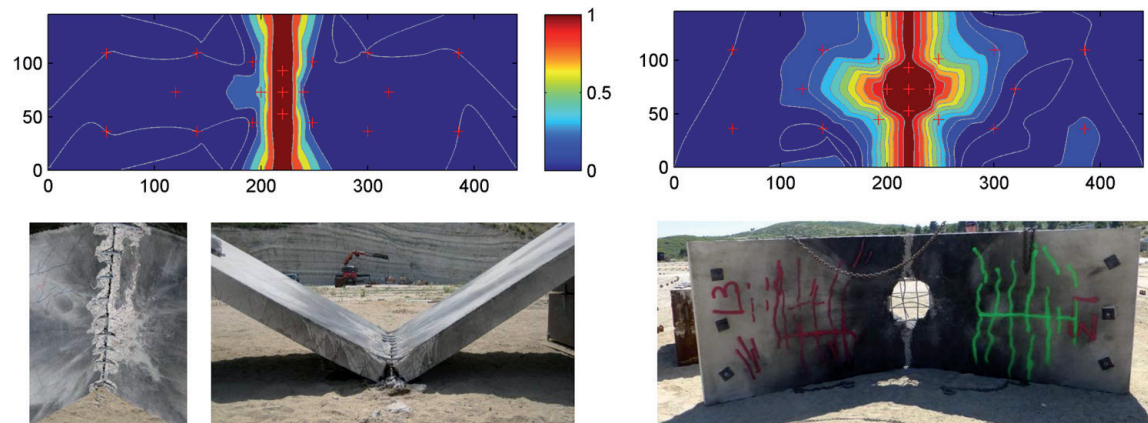


**Figure 8.**  
 Results for S4 and S8 tests and the comparison with damage maps. Z being the scaled distance.

While one of the two parameters is below 0.05, the damage is classified as no damage; no damage may denote appearance of little cracks, while concrete remains almost intact. If one of the parameters is above 0.05 and below 0.15, the damage is considered as moderate referring to specimens with important affected area and moderate to heavy concrete spalling. At last, if one parameter is above 0.15, the damage is severe considered as full spalling of the concrete thickness. Damage  $d_n$  has been evaluated at 19 points on the slab top surface. For slabs S1–S3, results were no damage. Only some little cracks appeared at the bottom face of slab S3. **Figure 8** shows the explosion effects on two slabs tested and the output from the damage maps.

As this methodology reflects, when reducing the scaled distance, damage  $d_{200}$  increases for slabs S1 to S5. These are the slabs without additional reinforcement. For slabs with steel sheet (S6 and S7), there is an increase of the area damaged in about 15 and 4%, respectively, when compared with the same configuration without steel sheet, S5. Nevertheless, the bottom part results defer up to 5%. At the same scaled distance, steel and polypropylene fibre slabs (S8 and S9), the evaluated damage  $d_{200}$  is almost the same compared with slab S5. Furthermore, when

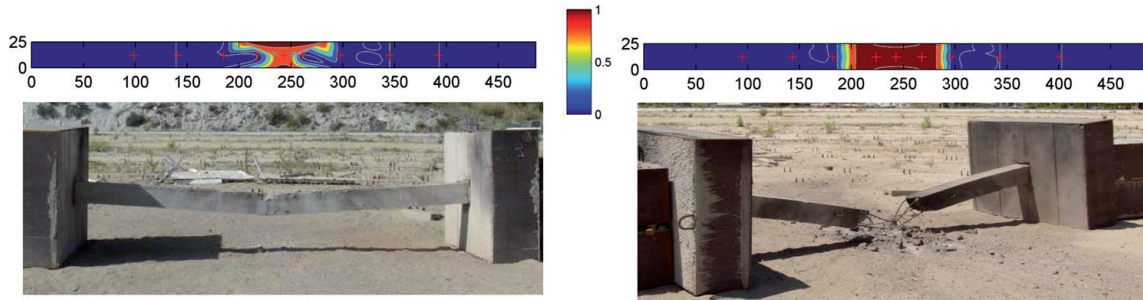


**Figure 9.**  
Results for B4 and B5 tests and the comparison with damage maps.  $Z$  being the scaled distance.

considering the area of damage on the top surface, the values are also very similar. However, at the bottom parts, the differences are noticeable.

**Table 5** also shows the data obtained after blast events over five beams tested. In this case, no additional reinforcement material was implemented in beams, so the study is only based on reinforced concrete (RC) beams. Damage  $d_n$  has been evaluated at 9 points on the top surface of the beam, which was the one exposed to the explosion. As in the slab test results, when the scaled distance decreases, all the damage parameters evaluated increase. Tests B1–B3 resulted in no damage after the evaluation. **Figure 9** shows the damage maps with some photos of the results for tests B4 and B5, with scaled distances of 0.41 and 0.20  $\text{m}/\text{kg}^{1/3}$ , respectively. In these tests, the only area damaged ( $d_A$ ) measured was the top surface (the surface directly exposed to the blast) due to the arrangement of the test, obtaining similar results as those with slabs for higher scaled distances.

In the numerical simulation, reinforced concrete slabs and beams were reproduced using 3D solid Lagrangian elements (using LS-DYNA software), while the explosive event is implemented with CONWEP. The steel rebar was incorporated into the concrete mesh using the LS-DYNA command: \*Constrained\_Lagrange\_in\_Solid. Using this feature, we assume a perfect bond, i.e., no sliding, due to short event time and high blast pressures. To save computational time, and taking advantage of the symmetry conditions, only one half along the major axis of each slab is considered. More details about the model can be found in Castedo et al. [15]. The explosive charge has been introduced into the model by the \*Load\_Blast\_Enhanced (LBE) function. This function is based on the Kingery-Bulmash empirical blast data [16]. The plasticity-based material model CSCM was used to simulate the concrete material in the slabs. The CSCM model has the option of inputting your own material properties or requesting default material properties for normal strength concrete introducing only the compressive strength  $f_c$  (**Table 4**). In this case, the second option was used. In this material type, the erosion is activated when its internal damage (plastic strain in LS-PrePost) reaches 99%. The steel bars were modelled using the piecewise linear plasticity material. This material model deals with the stress strain by a bilinear curve considering strain rate effects.

Results of numerical modelling can be used to compare the results of field tests, and if good agreement appears, results can be extrapolated to other cases without the need for verification by testing. As can be seen in **Figure 10**, models reproduce well the result of the field test. Furthermore, data extracted about area of damage are acceptable when compared with those measured in the field with errors up to 15% [17].

For beam modelling, considering the existing symmetry planes in the structure, and in order to reduce as much as possible the computational time, only a quarter of beam is created. It has been verified that the results for the models of a quarter with two symmetries, a half with a symmetry and the complete model give similar results.

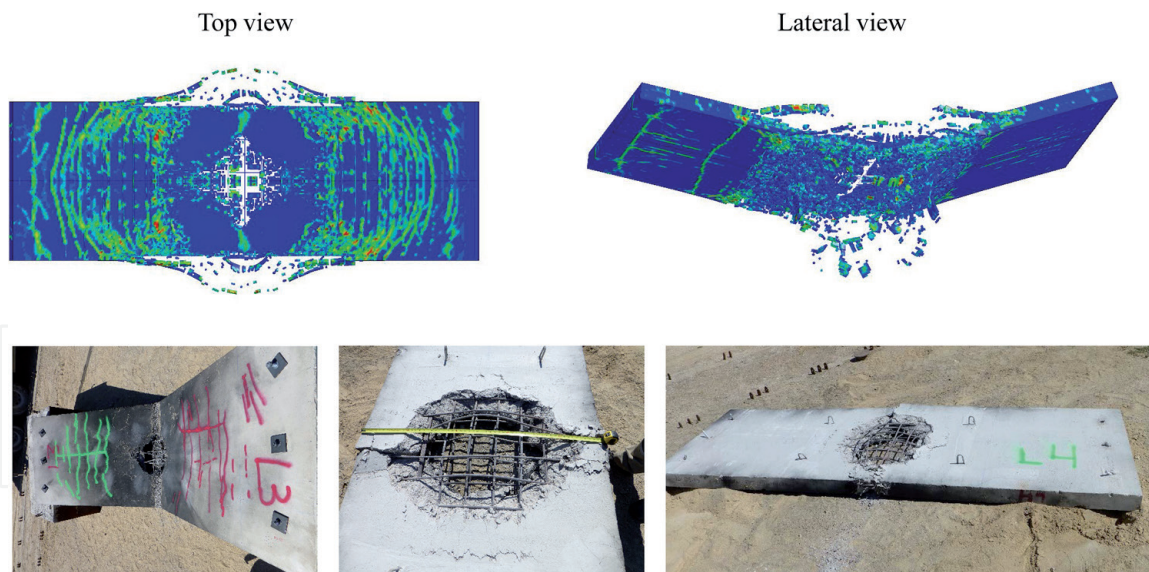


**Figure 10.**  
 Numerical modelling of S8 showing plastic strain and the comparison with the photographs of the test.

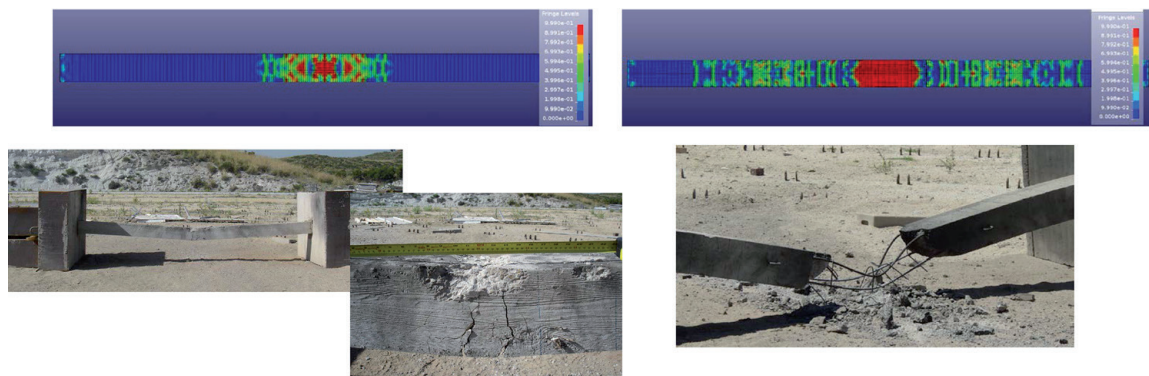


**Figure 11.**  
 Comparison of the numerical modelling for tests B4 and B5 and the test results.

The explosive charge has been introduced into the model in the same way that for slabs. Also, the same material models have been used for concrete and steel. **Figure 11** shows the plastic strain produced by the numerical modelling for beams B4 and B5 and the comparison with the photographs after the tests. As happened with the damage assessment and contour maps, results are in good agreement with those shown and measured in field tests.

### 3.3 Structural integrity

Once different structural elements and weak elements of a building have been tested, it would be desirable to know the behaviour of a complete structure subjected to a blast load. This kind of test is really difficult to implement due to the element dimension but mostly because of the high cost. In the test shown here, the behaviour of a frame structure after the removal by blasting of one of its columns is analysed experimentally, and the correspondence of this scenario to the theoretical calculation situation is checked. The structure analysed was a two-storey reinforced concrete structure. Each slab had dimensions of 14.35 m long by 11.00 m wide including this measure 2 metres of cantilever of the slab on each side of the structure. Each slab is supported by six reinforced concrete columns with a square section of 35 cm × 35 cm. The whole structure is built on site with reinforced concrete

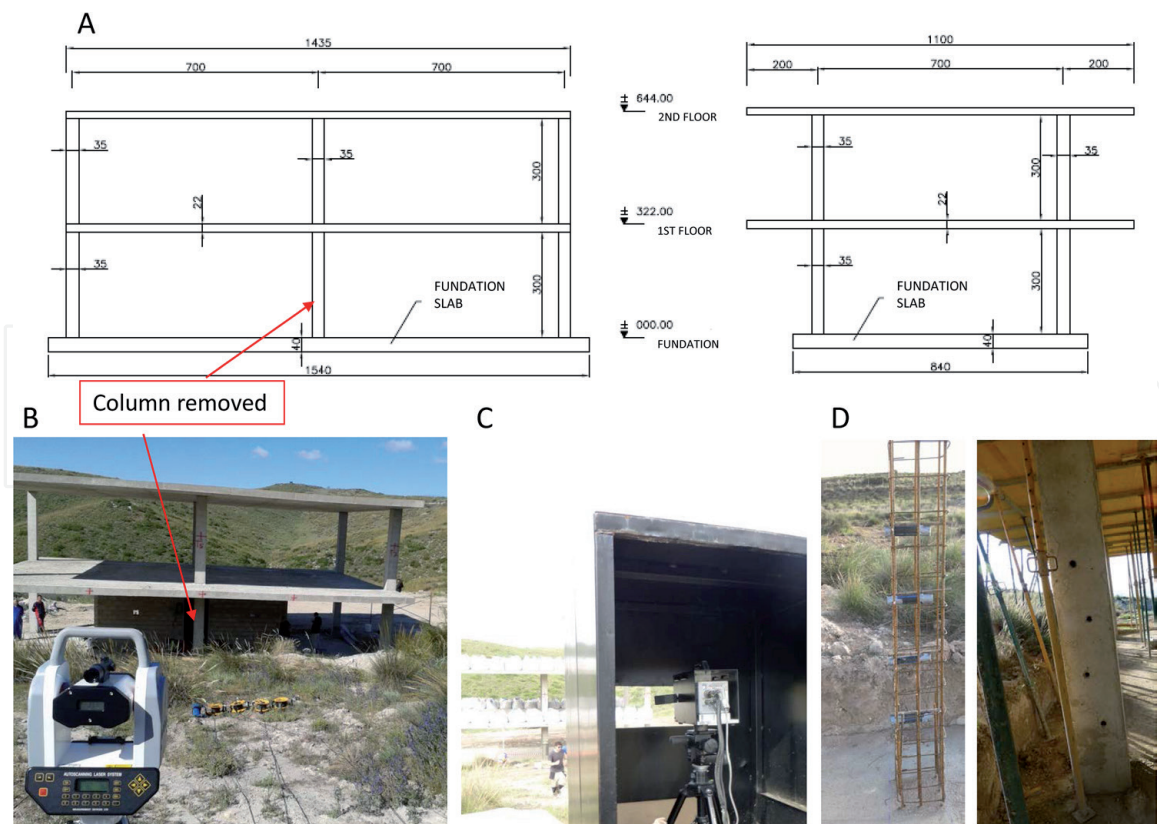


**Figure 12.**

(A) Geometrical details of structure. (B) Laser profiler used to measure the permanent strains. (C) High-speed camera. (D) Details of the column to be removed.

with a nominal characteristic compressive strength of 25 MPa and rebar with a yield strength of 500 MPa. **Figure 12** shows the constructive details.

The column to be instantly removed with explosives was one of the central columns of the main floor (see **Figure 12**). For the demolition of the column, four PG2 cylindrical loads of 200 g each were used. Insensitive instantaneous electric detonators were used and connected in series.

The test was monitored with the following equipment:

- Laser profiler: robotic total station that allowed to scan the structure and to evaluate the permanent strains.
- Accelerometers: four accelerometers connected to a fast acquisition system.
- Seismographs: recording of particle velocity (vibration) and air wave pressure (microphone). Three triaxial and one uniaxial geophones.
- High-speed cameras: analysis of the different phases of movement and evaluation of displacement and velocity. Two high-speed cameras were used.

### 3.3.1 Results and discussion

After the column was removed, the structure collapsed. The accelerometers and seismographs were trapped in the debris and could not record anything. No measure was possible with the laser profiler either, as there was no permanent strain after the collapse to be measured. The high-speed camera video made possible to evaluate the falling speed of the slab placed on the column removed. This measurement contributed to the calibration of the corresponding simulations.



**Figure 13.**  
*Sequence of the test recorded with a conventional camera.*

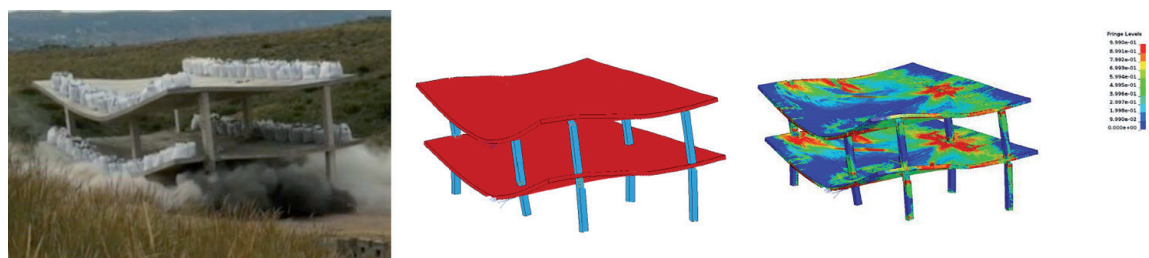


**Figure 14.**  
*Photograph of the structure collapse vs. 3D numerical model of the structure at time 1.1 seconds.*

The test was also recorded with two conventional cameras. **Figure 13** shows the sequence of the test with one of the cameras and the moment at which structure collapsed.

As the result of the test was the total collapse of the structure, no more information could be extracted apart from the visual data (videos recorded), hence the importance of achieving the intermediate level of damage in the trials. To reproduce and analyse the behaviour of the structure, numerical modelling was used. As in the previous cases of this work, a 3D model with Lagrangian mesh and CONWEP blast load description is developed. Also, the same material models (CSCM for concrete and piecewise linear plasticity material model for rebar) have been used. More details about the model are included in Bermejo et al. [18]. The models used for the reinforced concrete structure have proven their capacity to reproduce the complete process of the progressive collapse. **Figure 14** shows a frame from the video recorded at 1.1 seconds and the comparison with the numerical model at the same instant.

## 4. Conclusions

Several works with different constructive elements have been reported here. The complexity of the phenomena studied and the magnitude of the consequences highlight the great importance of the research in this field. For this purpose, only



numerical modelling is not acceptable, as there is a need of checking with real cases. Scale factor is another big problem, making it necessary to develop the tests at full scale. Furthermore, a good design of tests is essential to achieve an intermediate level of damage and, hence, to extract as much information as possible.

A total of 16 different tests have been carried out at full scale with different constructive elements. Finally, one test over a complete structure of a building has been developed and analysed. In most cases, numerical modelling and damage assessment have been made with the data extracted from the tests. In addition, numerical modelling of these tests can be used as a tool for predicting possible scenarios and analyse threats with similar conditions to those tested here.

## **Acknowledgements**

This research has been conducted under the SEGTRANS project funded by the Centre for the Development of Industrial Technology (CDTI), an agency of the Spanish government. We would like to thank TAPUSA, EUROESTUDIOS, KV Consultores and Sacyr, which contributed to the design and execution of the tests. We also would like to thank all the staff at La Marañosa (ITM-INTA) for their help at the testing site.

## **Author details**

María Chiquito\*, Anastasio P. Santos, Lina M. López and Ricardo Castedo  
E.T.S.I. de Minas y Energía. Universidad Politécnica de Madrid. Madrid, Spain

\*Address all correspondence to: [maria.chiquito@upm.es](mailto:maria.chiquito@upm.es)

## **IntechOpen**

© 2019 The Author(s). Licensee IntechOpen. This chapter is distributed under the terms of the Creative Commons Attribution License (<http://creativecommons.org/licenses/by/3.0>), which permits unrestricted use, distribution, and reproduction in any medium, provided the original work is properly cited. 

## References

- [1] Buchan PA, Chen JF. Blast resistance of FRP composites and polymer strengthened concrete and masonry structures – a state-of-the-art review. *Composites Part B: Engineering*. 2007;**38**(5):509-522
- [2] Silva PF, Lu B. Improving the blast resistance capacity of RC slabs with innovative composite materials. *Composites Part B: Engineering*. 2007;**38**(5):523-534
- [3] Tabatabaei ZS, Volz JS, Baird J, Gliha BP, Keener DI. Experimental and numerical analyses of long carbon fiber reinforced concrete panels exposed to blast loading. *International Journal of Impact Engineering*. 2013;**57**:70-80
- [4] Pantelides CP, Garfield TT, Richins WD, Larson TK, Blakeley JE. Reinforced concrete and fiber reinforced concrete panels subjected to blast detonations and post-blast static tests. *Engineering Structures*. 2014;**76**:24-33
- [5] Hajek R, Foglar M. Numerical and experimental analysis of the effect of rigid barriers on blast wave propagation. *Journal of Structural Engineering*. 2015;**141**:1-12
- [6] Schenker A, Anteby I, Gal E, Kivity Y, Nizri E, Sadot O. Full-scale field tests of concrete slabs subjected to blast loads. *International Journal of Impact Engineering*. 2008;**35**(3):184-198
- [7] López LM, Segarra P, Castedo R, Sanchidrián JA, Navarro J, Chiquito M. Performance of different constructive solutions against explosions in full-scale masonry walls. In: *Proceedings of the 11th International Symposium on Rock Fragmentation by Blasting*. Australia: Sydney; 2015
- [8] Chiquito M, López LM, Castedo R, Santos AP, Pérez-Caldentey A. Blast effects and damage characterization on reinforced masonry walls at full-scale. *WIT Transactions on The Built Environment*. 2018;**180**:113-123
- [9] Thiagarajan G, Kadambi AV, Robert S, Johnson CF. Experimental and finite element analysis of doubly reinforced concrete slabs subjected to blast loads. *International Journal of Impact Engineering*. 2015;**75**:162-173
- [10] Wang W, Zhang D, Lu F, Wang SC, Tang F. Experimental study and numerical simulation of the damage mode of a square reinforced concrete slab under close-in explosion. *Engineering Failure Analysis*. 2013;**27**:41-51
- [11] López LM, Sanchidrián JA, Piedra LJ, Rios J. Shock wave pressure in underground explosions. Explosives and blasting technique. In: Holmberg R, editor. *Proceedings of the EFEE 2nd World Conference*. Prague: Taylor & Francis; 2003. pp. 441-447
- [12] López LM, Castedo R, Chiquito M, Segarra P, Sanchidrián JA, Santos AP, et al. Post-blast non-destructive damage assessment on full-scale structural elements. *Journal of Nondestructive Evaluation*. 2019;**38**(1):30. DOI: 10.1007/s10921-019-0572-y
- [13] Department of the Army. *Structures to Resist the Effects of Accidental Explosions*, UFC 3-340-02. Washington, DC: U.S. Department of the Army, Navy and Air Force; 2008
- [14] Zhao CF, Chen JY. Damage mechanism and mode of square reinforced concrete slab subjected to blast loading. *Theoretical and Applied Fracture Mechanics*. 2013;**63**:54-62
- [15] Castedo R, Segarra P, Alañon A, Lopez LM, Santos AP, Sanchidrián JA. Air blast resistance of full-scale slabs with different compositions: Numerical

modeling and field validation.  
International Journal of Impact  
Engineering. 2015;**86**:145-156. DOI:  
10.1016/j.ijimpeng.2015.08.004

[16] Kingery CN, Bulmash G. Air Blast  
Parameters from TNT Spherical Air  
Burst and Hemispherical Surface Burst.  
Maryland: U.S. Army Ballistic Research  
Laboratory; 1984

[17] Castedo R, Lopez LM, Chiquito M,  
Santos AP. Full-scale reinforced  
concrete slabs: Blast effects, damage  
characterization and numerical  
modelling. International Journal of  
Safety and Security Engineering.  
2019;**9**(1):50-60. DOI: 10.2495/10.2495/  
SAFE-V9-N1-50-60

[18] Bermejo M, Santos AP, Goicolea JM.  
Development of practical finite element  
models for collapse of reinforced  
concrete structures and experimental  
validation. Shock and Vibration.  
2017;**2017**:9. DOI: 10.1155/2017/4636381